EARTH SURFACE PROCESSES AND LANDFORMS
Earth Surf. Process. Landforms **45**, 3702–3713 (2020)

Published online 15 September 2020 in Wiley Online Library
(wileyonlinelibrary.com) DOI: 10.1002/esp.4993

Width control on event-scale deposition and evacuation of sediment in bedrock-confined channels

Kristen L. Cook,[1]* Jens M. Turowski[1] and Niels Hovius[1,2]
[1] GFZ German Research Centre for Geosciences, Telegrafenberg, Potsdam, Germany
[2] Institute of Earth and Environmental Science, Potsdam University, Potsdam, Germany

Received 30 May 2020; Revised 11 August 2020; Accepted 26 August 2020

*Correspondence to: Kristen L. Cook, GFZ German Research Centre for Geosciences, GFZ Section 4.6, Telegrafenberg, 14473 Potsdam, Germany.
E-mail: klcook@gfz-potsdam.de

ESPL
Earth Surface Processes and Landforms

ABSTRACT: In mixed bedrock–alluvial rivers, the response of the system to a flood event can be affected by a number of factors, including coarse sediment availability in the channel, sediment supply from the hillslopes and upstream, flood sequencing and coarse sediment grain size distribution. However, the impact of along-stream changes in channel width on bedload transport dynamics remains largely unexplored. We combine field data, theory and numerical modelling to address this gap. First, we present observations from the Daan River gorge in western Taiwan, where the river flows through a 1 km long 20–50 m wide bedrock gorge bounded upstream and downstream by wide braidplains. We documented two flood events during which coarse sediment evacuation and redeposition appear to cause changes of up to several metres in channel bed elevation. Motivated by this case study, we examined the relationships between discharge, channel width and bedload transport capacity, and show that for a given slope narrow channels transport bedload more efficiently than wide ones at low discharges, whereas wider channels are more efficient at high discharges. We used the model sedFlow to explore this effect, running a random sequence of floods through a channel with a narrow gorge section bounded upstream and downstream by wider reaches. Channel response to imposed floods is complex, as high and low discharges drive different spatial patterns of erosion and deposition, and the channel may experience both of these regimes during the peak and recession periods of each flood. Our modelling suggests that width differences alone can drive substantial variations in sediment flux and bed response, without the need for variations in sediment supply or mobility. The fluctuations in sediment transport rates that result from width variations can lead to intermittent bed exposure, driving incision in different segments of the channel during different portions of the hydrograph. © 2020 The Authors. Earth Surface Processes and Landforms published by John Wiley & Sons Ltd

KEYWORDS: bedload transport; discharge variability; bedrock–alluvial channels; channel width; hysteresis

Introduction

Rivers are conveyer belts at the Earth's surface, moving large amounts of sediment across the landscape. At the same time, the amount of sediment is a key parameter controlling channel dynamics and geometry, with feedbacks on hydraulics and thus sediment transport capacity (Church, 2006; Recking *et al.*, 2008). Whether sediment deposition or entrainment occurs in a given river reach depends not only on local hydraulics, channel geometry and roughness, but also on the supply of sediment both from upstream and from adjacent hillslopes. In addition, in bedrock channels sediment supply affects bedrock erosion rates both by providing the tools for impact-driven erosion (the tools effect) and by shielding the rock from impacts in places where it is covered (the cover effect) (e.g., Sklar and Dietrich, 2004), and therefore controls the long-term adjustment of channel geometry to climatic and tectonic forcing conditions (Whipple, 2004).

In the concept of the graded stream, channel morphology tends to adjust such that the sediment load supplied from upstream can be transported without excess capacity (Mackin, 1948). In alluvial channels, the adjustment of channel width and slope can occur quickly, and the desired morphology can be achieved within a geomorphologically short time, sometimes even within a single flood. In contrast, in bedrock and mixed bedrock–alluvial channels, whereas slope can quickly adjust by deposition or removal of transient alluvial cover at least to some extent, the timescale for width changes is typically much longer than the return period of floods (e.g., Turowski, 2020). In general, channel width scales with discharge and sediment flux (Whipple, 2004;

Finnegan *et al.*, 2007; Yanites and Tucker, 2010; Whitbread *et al.*, 2015), but may also vary along a stream due to localized incision (e.g., Lavé and Avouac, 2001; Yanites *et al.*, 2010), differences in lithology and the strength of channel walls or banks (Montgomery and Gran, 2001; Eaton and Church, 2007; Bursztyn *et al.*, 2015), or recent slope failures (Korup, 2005; Ouimet *et al.*, 2008). While the concept of the graded stream is useful in understanding the long-term dynamics of river channels, it cannot be applied over short timescales, for example those of individual floods, where discharge and sediment supply can vary considerably (Bull, 1979; Turowski *et al.*, 2013). Particularly in bedrock channels, with their contrasting timescales governing sediment transport and channel geometry adjustment by bedrock erosion, there can be rich dynamic responses to rapid variations of discharge and sediment supply that may upscale to and influence channel dynamics on long timescales, but are often overlooked.

Variations in bedload transport rates over the course of single floods have been observed in many settings, commonly in the form of hysteresis in the discharge–bedload transport relationship (Nanson, 1974; Reid *et al.*, 1985; Gomez, 1991; Kuhnle, 1992; Turowski *et al.*, 2009; Mao *et al.*, 2014; Roth *et al.*, 2014). Typically, this variability is explained by temporal changes in sediment supply (Nanson, 1974; Habersack *et al.*, 2001; Mao *et al.*, 2014), bedform dynamics (Gomez *et al.*, 1989; Hoey, 1992), sediment waves (Meade, 1985; Hoey, 1992; Roth *et al.*, 2014) and/or changes in sediment mobility due to bed armouring (Gomez, 1983; Reid *et al.*, 1985; Kuhnle, 1992). Within this contribution, we explore another potential control on bedload transport variability and hypothesize that along-stream channel width variations can lead to spatial and temporal variations in bedload flux. While width changes have long been recognized as an influence on equilibrium channel geometry and sediment transport, particularly in the engineering community (Davies and Lee, 1988; Griffiths and Carson, 2000; Mueller and Wagner, 2005; Yanites and Tucker, 2010; Sturm *et al.*, 2011), we propose that they can also drive short-term variability, leading to complex patterns of sediment entrainment and deposition and changes in bed elevation at both the intra-flood and inter-flood timescales.

We motivate this hypothesis using a case study from the Daan River gorge (Cook *et al.*, 2013, 2014), where we observed substantial changes in bed elevation during flood events in a section of the river with large differences in channel width due to localized bedrock confinement. We then explore the influence of spatial variations in channel width on bedload transport using both theoretical analyses and numerical simulations with the sediment transport model sedFlow (Heimann *et al.*, 2015a, 2015b).

Field Observations

The Daan River is located in western Taiwan, extending from the 3 km high Hsueshan Range west to the Taiwan Strait (Figure 1). Where the river crosses the frontal structures of the Hsueshan Range, coseismic uplift in the riverbed during the 1999 Chi-Chi earthquake resulted in the formation of a narrow bedrock gorge bounded upstream and downstream by wide braidplains with an average slope of 0.014 (Cook *et al.*, 2013, 2014). While the flow width in the braidplain can vary with discharge, the total width of the braidplain is set by the bedrock on one side and a floodwall on the other. The channel abruptly changes in width through this reach, narrowing from up to several hundred metres in the upstream braidplain to ~20 m as it enters the 1 km long gorge, and then widening from ~40 m back

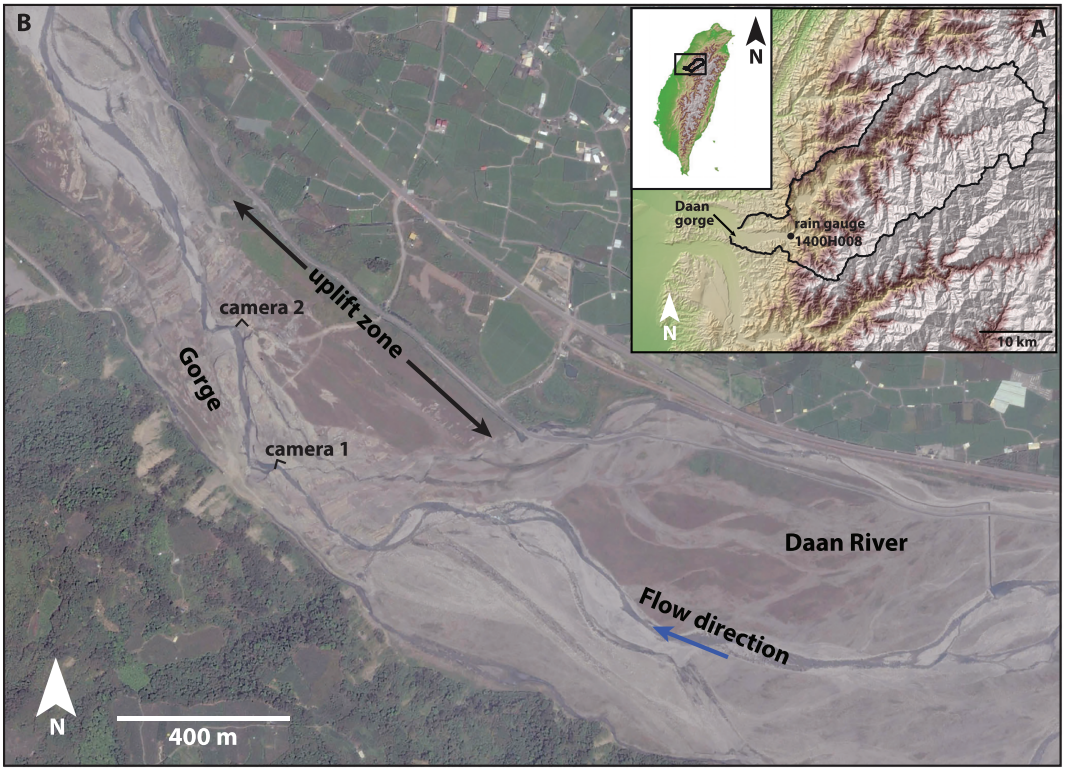

Figure 1. Location and overview of the Daan River field site. (A) Outline of the Daan River catchment. Elevations reach up to 3800 m at the eastern drainage divide. The black circle shows the location of the Taiwan Water Resources Agency (WRA) rain gauge for the reported precipitation values. Inset shows the location of the Daan catchment on the island of Taiwan. Modified from figure 1 of Cook *et al.* (2013). (B) Google Earth image of the Daan River gorge on 20 April 2011, showing the geometry of the channel prior to the 2012 floods. The locations and view directions of the time-lapse cameras are shown. [Colour figure can be viewed at wileyonlinelibrary.com]

to up to several hundred metres at the downstream end of the gorge (Figure 1).

The Daan River has highly variable flow, with spring monsoon and typhoon floods increasing the discharge by up to several orders of magnitude above the background discharge of 5–10 m^3 s^{-1}. Bedload transport occurs only during flood conditions and the bed is stable at background discharges. This assessment is based on field observations from 58 visits to the gorge between 2009 and 2019, including direct observation of the channel bed during low flow conditions on multiple occasions, as well as the development and preservation of biofilms in the channel bed over weeks to months of low flow conditions. Bedload in the gorge and adjacent regions has a D_{50} of 0.10 m, D_{16} of 0.03 m and D_{84} of 0.25 m (based on point counts from bars and sections through recent deposits) and is dominated by quartzite clasts sourced from Eocene and Oligocene rocks more than 28 km upstream (Cook *et al.*, 2013). Less than ~5% of the bedload is made up of the local sandstone and mudstone bedrock of the Plio-Pleistocene Cholan Formation. For more than 20 km upstream of the gorge, the river occupies a wide braidplain with abundant coarse sediment and little to no bedrock exposure. The lack of locally sourced clasts in the bedload and ample upstream bedload storage suggests that bedload supply for a given flood is not related to concurrent hillslope processes.

The evolution of the Daan River gorge has been documented in detail by Cook *et al.* (2013, 2014). Briefly, a section of the riverbed about 1 km long was uplifted by up to 10 m during the 1999 Chi-Chi earthquake. Incision through the uplifted topography was initially hindered by a lack of bedload tools, but in 2004 gorge initiation began at the downstream end of the uplift zone. The gorge grew rapidly upstream via knickpoint retreat. In 2008, incision reached the upstream end of the uplift zone, resulting in a 1 km long bedrock gorge up to 20 m deep with near-vertical to vertical walls. Bedrock has not been observed in the bed of the gorge since 2010. By 2012, downward bedrock erosion in the gorge had ceased and the bed was mantled by at least 5 m of alluvium with an average slope of 0.011 through the gorge. Changes to the channel since this time are related to the deposition and removal of alluvium, along with minor lateral bedrock erosion.

We used time-lapse cameras to record the behaviour of the channel both between and during flood events. We installed two Moultrie Gamespy cameras above the channel in June 2011, with camera 1 overlooking an 11–30 m wide reach in the upstream portion of the gorge and camera 2 overlooking a

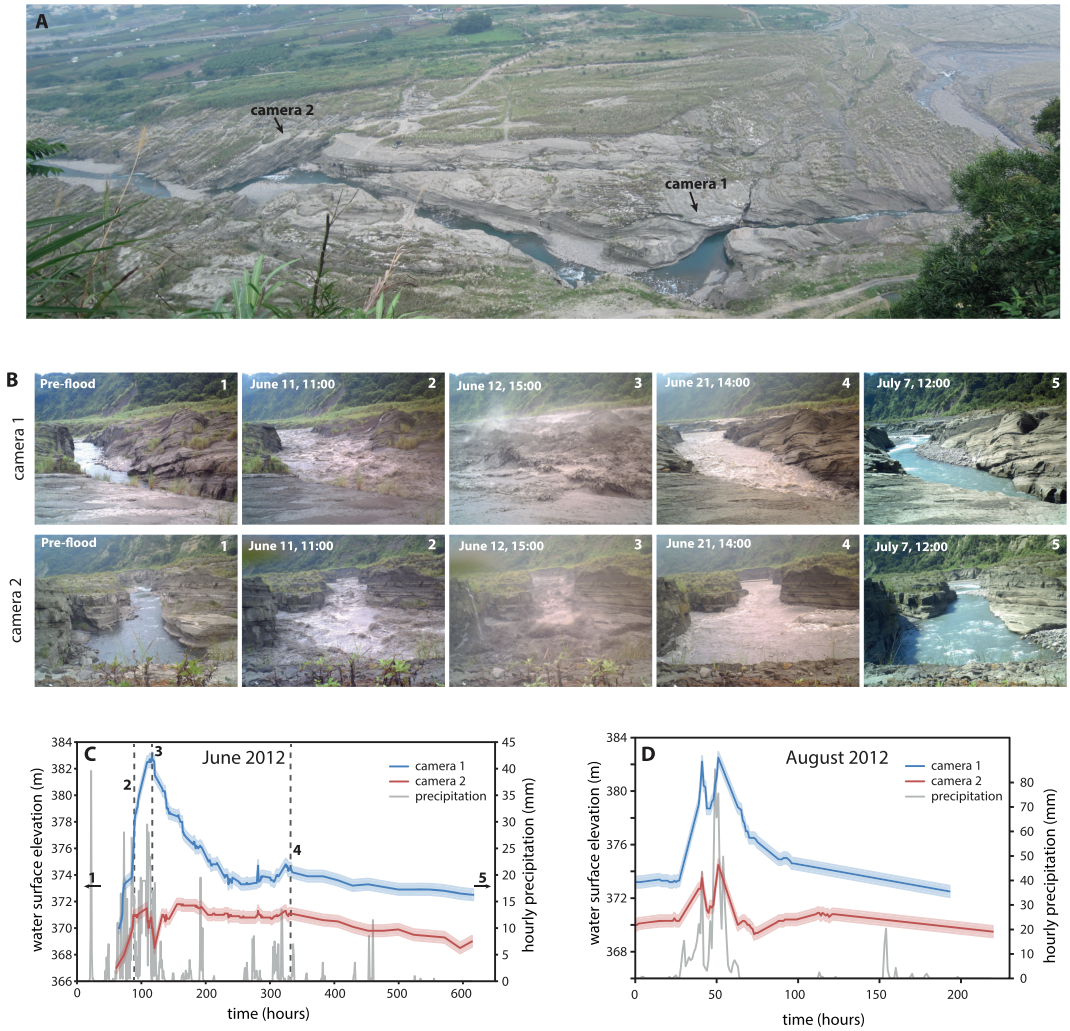

Figure 2. Time-lapse camera observations. (A) Overview of the Daan River gorge, showing the locations of cameras 1 and 2. Both cameras are looking upstream. The scale varies in this photograph, but cameras 1 and 2 are about 300 m apart. (B) Time-lapse photographs from the June 2012 flood. (C) Water surface elevation estimated from the photographs and hourly precipitation for the June 2012 flood. Black dashed lines and numbers show the time of the photographs in (B). Shading shows uncertainty bounds of ±0.5 m. (D) Water surface elevation estimated from the photographs and hourly precipitation for the August 2012 flood. Precipitation data in (C) and (D) are from Taiwan WRA Shuangqi station (1400H008), located 8 km upstream of the gorge. [Colour figure can be viewed at wileyonlinelibrary.com]

reach up to 75 m wide in the downstream portion of the gorge (Figure 2). The cameras are about 300 m apart, and there are no tributaries between the two locations, so the discharge in these gorge sections is the same, unless the gorge walls are overtopped. Each camera was set to take two photographs (one approximately 10 s after the other) every hour. Water surface elevations were estimated from the photographs using reference elevations based on terrestrial LiDAR scans of the gorge walls conducted at centimetre resolution with a Riegl VZ-1000 scanner (Cook *et al.*, 2014). The dominant source of uncertainty is the difficulty in precisely defining the water surface during periods of high turbulence. To account for this, we assign a conservative uncertainty of ±0.5 m to all water surface elevations. The light proved insufficient for night-time photographs, so only daytime water-level data could be constrained. As water surface elevation is controlled by both flow depth and the thickness of alluvium on the channel bed, changes in water level may provide insight into local erosion and deposition during the course of a flood. The cameras operated for 2 years before they were destroyed by a flood in 2013; during this time, two large flood events occurred, both during the summer of 2012. Floods such as these are not exceptional for the Daan River, occurring approximately every 1–2 years on average.

The first flood, which began on 11 June 2012, was caused by spring monsoon precipitation of 806 mm over 8 days, as measured at Taiwan Water Resources Agency station 1400H008, located 8 km upstream of the gorge. This flood was net depositional, with before-and-after photographs at low flow showing aggradation of ~2 m in both photographed reaches. Over the course of the flood, the upstream reach (camera 1) showed a typical stage hydrograph, as water surface elevation increased to a maximum of ~12.5 m above the starting level over 54 h, and then decreased to background levels over the course of several weeks. Water levels were consistent with the apparent strength of the flood based on the evidence of turbulence in the photographs (Figure 2). In contrast, the downstream reach (camera 2) showed a more complicated stage hydrograph, with an initial increase in water surface elevation over 30 h, followed by an 18 h long period of little change, a decrease in the water surface elevation during the most turbulent portion of the flood, an increase in water surface elevation to reach a maximum as the flood abated, another period of little change for about 100 h, and finally a slow decline in water surface elevation (Figure 2). The maximum water surface elevation recorded at camera 1 coincided with a water surface elevation low recorded at camera 2, and the maximum water surface elevation at camera 2 occurred 44 h after the maximum at camera 1. In general, the two stage hydrographs were not correlated over much of the flood. As discharge is the same at both locations, the observed discrepancy in water surface elevation between the reaches could only result from changes in the bed elevation. This required a significant amount of sediment excavation and deposition in the reach covered by camera 2 during the course of the flood, as the water surface elevation declined by ~3 m during the middle of the flood.

The second flood, which began on 1 August 2012, was associated with the passage of typhoon Saola, with a total of 582 mm of precipitation over 8 days. This flood had a slight net erosional effect, with before-and-after photographs showing minor (<0.25 m) lowering in each photographed reach. In comparison to the flood in June 2012, the discharge was much flashier, with the water level in both reaches responding rapidly to local rainfall (Figure 2). Both reaches had an initial peak in water level followed by a decline and then a second peak. Following this second peak, the water level at camera 1 declined monotonically. In contrast, the water level at camera 2 declined for 22 h, then increased by about 1.5 m over the course of 42 h before steadily declining over the rest of the flood. We cannot distinguish between water-level changes due to changes in discharge and those due to bed elevation changes until the waning stages of the flood, when the downstream reach (camera 2) experienced a water-level low and subsequent rise that was asynchronous with the upstream reach (camera 1). This water-level rise, coincident with apparent decreasing discharge, must have been due to deposition on the bed.

The reach photographed by camera 2 experienced significant changes in bed elevation during both floods. The apparent erosion and deposition that we infer from water surface elevation observations during the floods are not consistent with the observed net change to the bed – during flood 1 we infer phases of bed erosion, but overall the bed aggraded. During flood 2 we infer phases of deposition of at least 1.5 m, but the net change of bed elevation was erosional. Fluctuations in bed elevation during these events may therefore have been much larger than can be constrained by before-and-after surveys of the channel. Meanwhile, we are unable to identify episodes of intra-flood bed elevation change in the reach photographed by camera 1. This reach is narrower, so the same change in discharge results in a larger variation in water depth, which may overprint any signal of bed elevation change. In addition, a signal of bed aggradation during a flood peak and bed erosion during flood recession would be impossible to distinguish from the stage data without reliable discharge data from a stable cross-section, which is lacking in the Daan River.

These observations motivate the question of what could drive these large, and potentially spatially variable, changes in bed elevation over the course of flood events. While a number of factors will affect sediment transport and erosion and deposition patterns during floods, we hypothesize that one potential driver of these changes could be complications in sediment dynamics induced by the combination of large temporal variations in discharge and large spatial variations in the width of the Daan River channel at the entrance and exit of the gorge reach. In order to test this hypothesis, we explore the possible impact of channel width on sediment transport both theoretically and through numerical modelling.

Width Variation and Bedload Transport Capacity

Local flood hydraulics, and therefore bedload transport capacity, depend on channel geometry, typically quantified by channel width and bed slope. Conventionally, bedload transport capacity is thought to depend on excess shear stress, which is related to channel geometry via slope S and the hydraulic radius R. The dimensionless shear stress τ^* is given by

$$\tau* = \frac{\rho_w}{\rho_s - \rho_w}\frac{SR}{D_{50}} \quad (1)$$

Here, D_{50} is the median grain size, and ρ_w and ρ_s are the densities of water and sediment, respectively. For a rectangular channel, the hydraulic radius can be rewritten in terms of channel width w and flow depth d as

$$R = \frac{wd}{w + 2d} \quad (2)$$

Using the formulation of Fernandez-Luque and van Beek (1976), bedload transport capacity can be given by

$$q_t = 5.7\rho_s\left(\frac{\rho_s - \rho_w}{\rho_w} g D_{50}^3\right)^{1/2} (\tau* - \tau*_c)^{3/2} \quad (3)$$

where τ^*_c is the dimensionless critical shear stress for bedload entrainment, which we set to 0.045 for all calculations.

For a given slope and grain size, Equation 3 reduces to

$$q_t = k_1(k_2 R - \tau*_c)^{3/2} \quad (4)$$

Here, k_1 and k_2 are constants when slope, grain size, and water and sediment densities are uniform. The hydraulic radius can be related to discharge Q_w using the Manning equation:

$$Q_w = \frac{1}{n} A R^{2/3} S^{1/2} \quad (5)$$

where A is the channel cross-sectional area, and n is Manning's roughness coefficient, which we set to 0.04 for all calculations.

From Equations 4 and 5, the bedload transport capacity per unit width, q_t, increases as the channel narrows until it reaches a peak and then declines with further narrowing (Figure 3A). As Equation 4 indicates, this dependence is controlled by the hydraulic radius of the channel. Where the channel is much wider than the flow depth, R is approximately equal to flow depth, which decreases with increasing width, leading to the reduction of shear stress and transport capacity. In the other extreme, where the channel is narrow, flow depth may be much greater than width, leading to the approximation $R = w/2$. Then, as the effects of friction on the channel walls become more significant, shear stress and transport capacity decrease as width decreases. The location of the peak between these two regimes is affected by the balance of flow depth and width, and therefore by the discharge. As discharge increases, the peak occurs at increasing values of width, for channels with a rectangular cross section (Figure 3A).

To obtain the total bedload transport capacity, Q_t, Equation 4 is multiplied by channel width (Figure 3B). As with the unit bedload transport capacity, for a given discharge there is a channel width at which Q_t reaches a maximum (Carson and Griffiths, 1987) and this peak in Q_t is dependent on discharge, and occurs at larger widths as discharge increases. At low discharges, Q_t is highest for narrow channels and slowly decreases with increasing width. However, at higher discharges, Q_t increases rapidly with increasing width and then slowly declines, as the decrease in bed shear stress with increasing width is partly compensated by the increased bed area available for sediment transport (Figure 3B).

This analysis shows that the relative efficiency of total sediment transport for channels of different widths is dependent on discharge (Figure 4A). At low discharges, narrow channels have a higher transport capacity than wide ones with the same bed slope, but the situation reverses at high discharges and the transport capacity of the wider channel becomes higher. The definition of 'high' and 'low' discharges, and the point at which the transport capacities reverse, can vary considerably. For a given slope and grain size, a pair of channel widths has one discharge at which they have the same transport capacity: the crossing point of the transport capacity–discharge relationships for each width (Figure 4A). This crossing point provides information about the discharges at which width variations may be important. The discharge crossing point depends on bed slope and grain size, as well as the two width values. In general, crossing point discharges decrease with decreasing D_{50} and increasing slope, so higher transport capacity for a given discharge leads to smaller crossing point discharges (Figure 4).

So far, we have discussed the relationship between transport capacity and channel width for a channel with uniform bed slope. In a natural system, if a channel has both narrow and wide reaches, the channel slope can adjust by local deposition or entrainment of sediment until transport capacity is the same everywhere. This has long been recognized, and can be observed when a channel is artificially narrowed by engineering activities (Richardson and Davis, 1995; Mueller and Wagner, 2005; Sturm *et al.*, 2011). However, the slopes necessary to achieve uniform sediment transport through reaches of different width depend on discharge. At low discharge, high transport capacity in a narrow reach results in a lower equilibrium slope there relative to a wide reach. At high discharge, a narrow reach must have a steeper slope to counteract the reduced transport capacity relative to a wide reach. Therefore, in order to maintain grade as discharge in the river changes through time, the reaches of different width need to adjust their relative slopes in response, leading to sediment erosion and aggradation and bed elevation changes. During a flood, discharge varies continuously and substantially, causing the channel to continuously adjust its slope in response. Even if this adjustment is not complete on the timescale of flood discharge variations, we can expect the elevation of the channel bed to fluctuate over the course of the flood. In real rivers, the effect of varying transport capacity may be combined with other processes related to rapidly changing width, such as backwater development or other hydrodynamic changes.

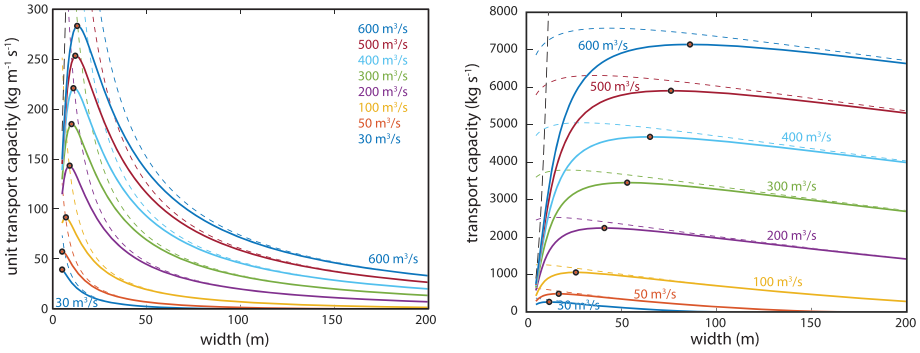

Figure 3. Bedload transport capacity versus width for discharges ranging from 30 to 600 $m^3\ s^{-1}$. (A) Unit transport capacity. (B) Total transport capacity. Solid lines show calculations using Equations 1-4; coloured dashed lines show capacity using a wide channel approximation (hydraulic radius equals flow depth); the black dashed line shows capacity using a narrow channel approximation (hydraulic radius equals width/2). Black points indicate the maximum transport capacities for each discharge. All calculations used a slope of 0.015 and grain size of 0.05 m. [Colour figure can be viewed at wileyonlinelibrary.com]

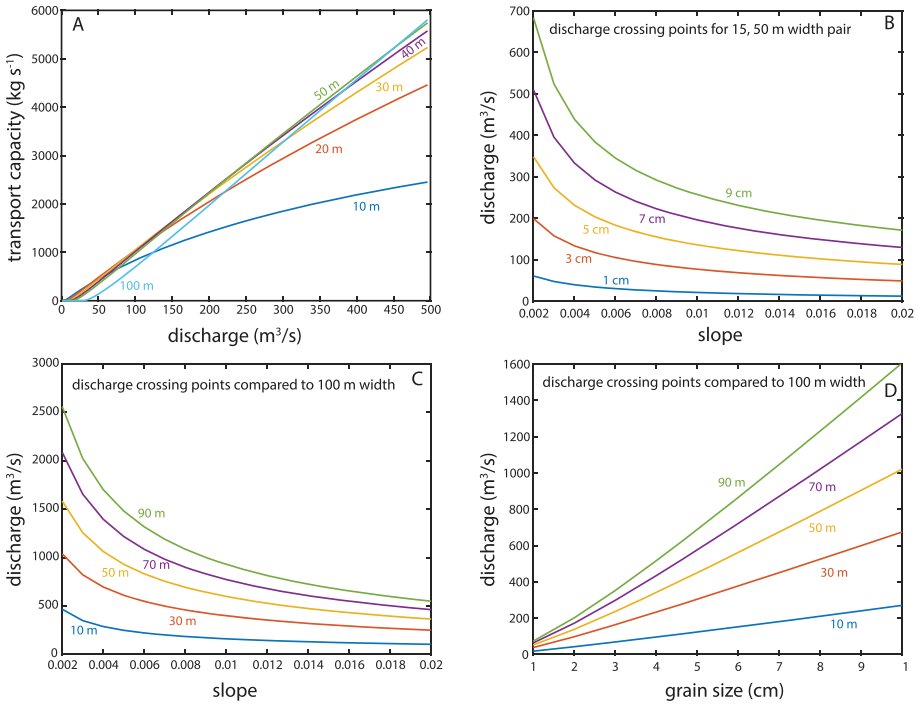

Figure 4. Transport capacity–discharge crossing point relationships. (A) Transport capacity versus discharge for different widths, calculated with a slope of 0.015 and grain size of 5 cm. (B)–(D) Plots of crossing point discharges: the discharge at which the transport capacity is equal for two reaches of different width. (B) Crossing point discharge versus slope for the width pair 15 m and 50 m. Each line shows the calculation for a different grain size. (C) Crossing point discharge versus slope; each line shows the calculation for a different width paired with a 100 m wide channel; calculated with grain size of 5 cm. (D) Crossing point discharge versus grain size; each line shows the calculation for a different width paired with a 100 m wide channel; calculated with slope of 0.015. [Colour figure can be viewed at wileyonlinelibrary.com]

Numerical Modelling

Motivated by the above theoretical considerations, we use the model sedFlow (Heimann *et al.*, 2015a) to further explore the effect of width variation on a river's response to floods of various magnitudes. sedFlow is a 1-D model of bedload transport and long profile evolution suitable for modelling transport at the event scale and the reach scale. It does not model hydraulics in detail, but takes a cross-section average approach. The model is adaptable and can incorporate different methods of calculating flow resistance, flow routing and bedload transport, as well as grain size distributions and fractional transport. The formulations that we used are specified in the model setup below. The model allows for erosion and deposition of bed material, but the channel width remains fixed. Details of the model can be found in Heimann *et al.* (2015a). sedFlow has been validated by comparison with data from several Swiss mountain rivers (Heimann *et al.*, 2015b).

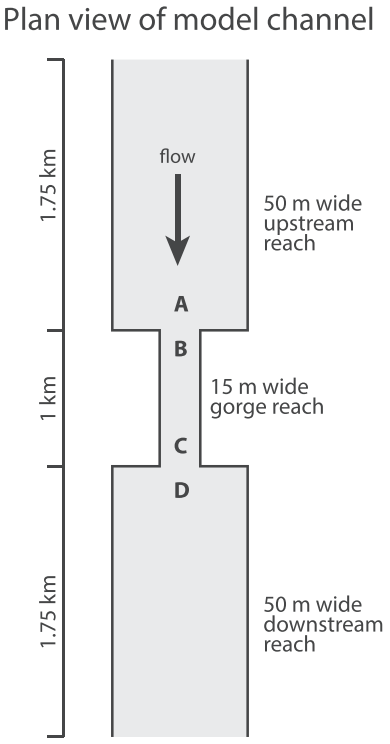

Figure 5. Plan view of model channel. Letters indicate the points for which results are shown in subsequent figures.

Model setup

To isolate the effect of width variation, we used a simple reach-scale channel configuration, with parameters motivated by the Daan River field case. We ran the model in a 4.5 km long channel, the centre of which contains a 1 km long gorge section with a width of 15 m, bounded upstream and downstream by 1.75 km long sections with widths of 50 m (Figure 5). Each section of the channel had a rectangular cross-section with a fixed width, and a bed with infinitely deep sediment, approximating a bedrock-walled channel with an alluvial bed. As a control, we also ran the model in a channel with a uniform width of 50 m.

Discharge was imposed at the upstream end of the model reach and was the only input varied. Flow routing was based on the implicit method of Liu and Todini (2002), and flow resistance was calculated using the grain-size dependent Manning–Strickler relationship. We created a discharge time series based

on a scaled unit hydrograph (SCS, 1972), where each flood consisted of the unit hydrograph scaled a peak discharge and a timescale. For each flood, we obtained the peak discharge by first randomly selecting from an exponential distribution with a mean of 250 $m^3\ s^{-1}$, and then adding 50 $m^3\ s^{-1}$ to the randomly selected value to impose a minimum flood magnitude of 50 $m^3\ s^{-1}$. The timescale for each flood was generated by randomly selecting from a uniform distribution between 0.5 and 1.5 days, and then modulating by the peak discharge for that flood, so that larger floods were biased towards longer timescales. Each flood began and ended at the same baseflow value of 1 $m^3\ s^{-1}$, a discharge at which no bedload transport is possible. The discharge series consisted of a sequence of these floods. In order to reduce processing time, we did not include periods of base flow between floods, during which no channel changes occur. We initially created a channel with a uniform slope of 0.015, ran a sequence of 30 randomly generated floods through this channel and used the resulting longitudinal profile as the input for all model runs. We then ran the model for two different randomly generated sequences of 50 floods each. For a second control case, we also ran a series of identical floods with peak discharge of 500 $m^3\ s^{-1}$ through the gorge model.

Sediment flux was based on the Rickenmann bedload transport equation (Rickenmann, 2001) with a dimensionless critical shear stress of 0.045, and we used a single grain size (either 3, 5 or 7.5 cm gravel) for the bedload. Sediment input into the model was based on the transport capacity of a representative upstream reach. The slope and width of this reach were taken from the upstream end of the input longitudinal profile and were kept constant throughout the model run. As a result, sediment input into the modelled reach depended only on the imposed discharge. We assume that the bed is entirely alluvial throughout the model, so that bedload transport can always reach the local transport capacity.

Model results

In the uniform width control case, each flood causes uniform bedload transport through the model reach, and therefore there is no net erosion or deposition and no change in bed elevation. The magnitude or duration of the floods has no impact on the channel morphology. For the repeating flood control case, after a period of adjustment, the channel longitudinal profile reaches a steady pattern. The bed elevation changes within each flood, but recovers back to its original position by the end of the flood, so there is no net change (Figure 6).

In contrast to the above control cases, the models with both width and discharge variation lead to a channel that responds to the imposed floods in complex ways (Figure 7). At high discharges, the narrow gorge reach transports less total sediment than the wide reaches, leading to aggradation in the upper part of the gorge and the wider section upstream, and erosion in the lower part of the gorge and the wider section downstream. At lower discharges, the gorge becomes more efficient at transporting sediment and the trends reverse (Figure 8). Small floods encourage a reduction of slope within the gorge reach, but these floods are often unable to transport sufficient sediment to reach their equilibrium slope. As a result, a sequence of small floods tends to monotonically drive deposition at the upstream end of the gorge and erosion at the downstream end (Figure 7). In contrast, large floods are able to transport sufficient sediment to drive large adjustments to the channel, but their net impact is highly dependent on the flood duration. Lower discharges in the tails of floods reverse the patterns of erosion and deposition caused by the high discharges during the flood peak. Therefore, the length of the recession determines the degree to which the low discharges in the tail can transport enough sediment to adjust the channel slope. The maximum of bed elevation change does not occur at the flood peak, but lags behind the time of maximum discharge.

The net change in bed elevation for each flood, defined as the difference between bed elevation at the start and end of each flood, is highly variable, both in the magnitude of the change and in whether the flood is erosional or depositional (Figure 9A). While there is a general trend for large floods to be net depositional at the upstream end of the gorge (i.e., point B) and net erosional at the downstream end of the gorge (i.e., point C), this is not always the case, as the net change is also influenced by flood sequencing and the duration of the flood. In the wider reaches upstream and downstream of the gorge (points A and D), the net change is even more variable and has no apparent trend with peak discharge.

The intra-flood change for each flood, defined as the difference between the starting elevation and either the maximum or minimum bed elevation within each flood period, shows more consistency with flood size, particularly for the gorge sections (Figure 9B). Intra-flood change tends to increase in magnitude with increasing peak discharge, but some variability related to flood duration and prior conditions remains. At peak discharges above 200 $m^3\ s^{-1}$, the maximum intra-flood change becomes consistently depositional in the upstream section (point B) of the gorge, and consistently erosional in the downstream section (point C). The sections upstream and downstream of the gorge (points A and D) remain more variable, and only become consistently depositional or erosional at peak discharges around 600 $m^3\ s^{-1}$. The relationship between net change and intra-flood change varies with flood size (Figure 9C). For the smallest floods, the net change and

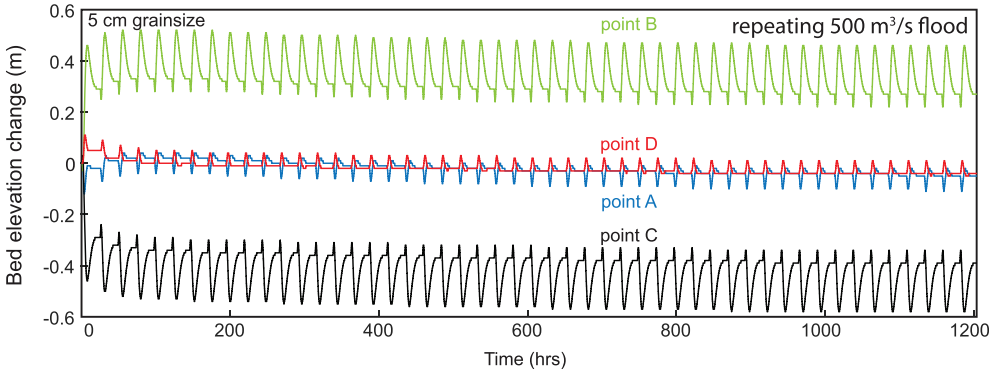

Figure 6. Modelled bed elevation changes (relative to initial bed elevation) for control case with a repeating flood of 500 $m^3\ s^{-1}$. [Colour figure can be viewed at wileyonlinelibrary.com]

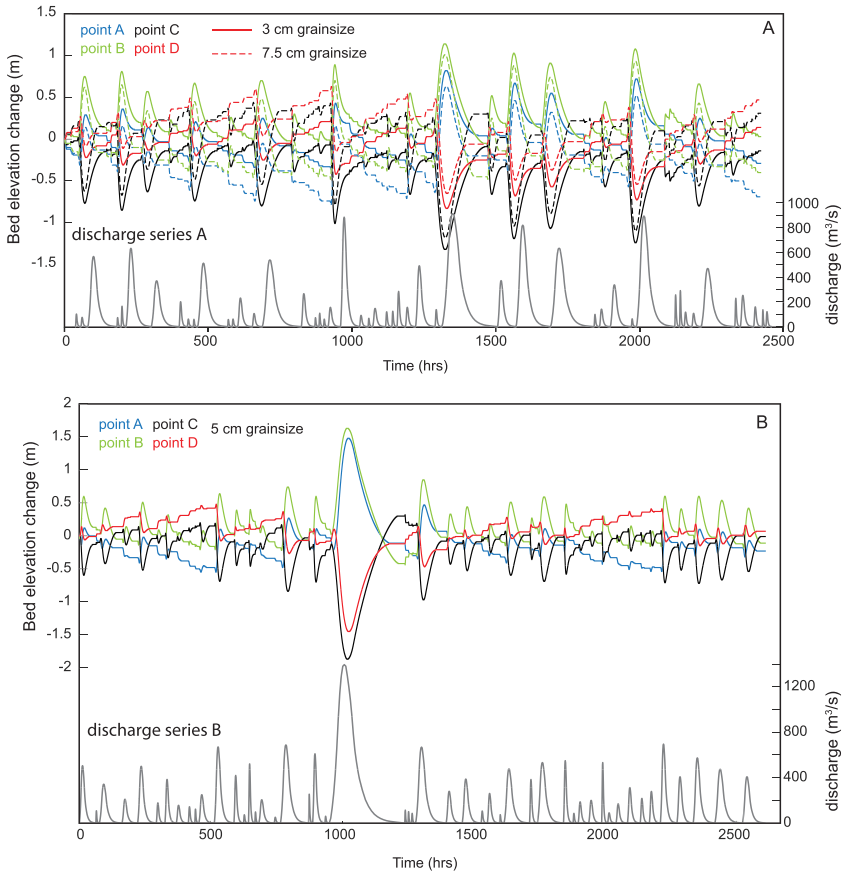

Figure 7. Modelled bed elevation changes (relative to initial bed elevation). (A) Model results for discharge time series A run with two different grain sizes. Grey line shows the input discharge. Bed elevation changes are colour-coded for the four locations in the channel shown in Figure 5. Solid lines show results for a grain size of 3 cm; dashed lines show results for a grain size of 7.5 cm. (B) Model results for discharge time series B and a grain size of 5 cm. [Colour figure can be viewed at wileyonlinelibrary.com]

intra-flood change is the same. However, for all other floods, net change is a poor predictor of intra-flood changes. The difference between the two tends to increase with increasing flood size; however, variability due to flood duration and sequencing remains (Figure 9D).

As discussed above, the bedload grain size influences the crossing point of the transport capacity–discharge functions for different widths, so for a given discharge distribution a change in grain size changes the distribution of erosive versus depositional events in each section. Grain size also affects the total transport capacity, which influences how quickly a reach can adjust to a change in discharge. Smaller grain sizes lead to more rapid adjustment and larger changes at high flow, but smaller cumulative changes during series of small flood events (Figure 7).

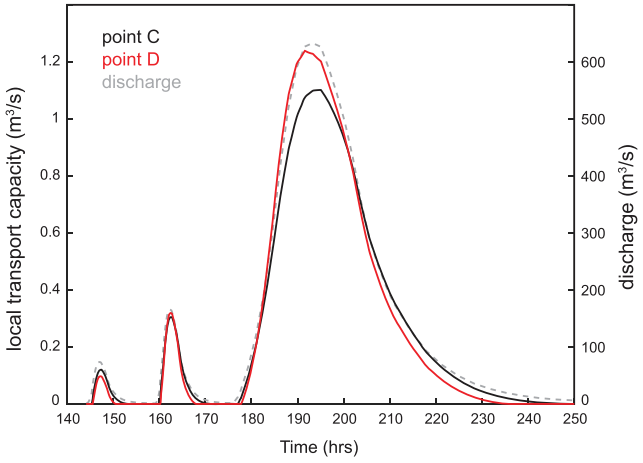

Figure 8. Bedload transport capacity at points C and D over the course of three floods (floods 4–6 of discharge time series A, grain size of 5 cm). Grey dashed line shows the discharge. [Colour figure can be viewed at wileyonlinelibrary.com]

Discussion and Implications

While our data from the Daan gorge are limited, our observations of apparent bed elevation changes during the two observed floods are consistent with model predictions. The apparent erosion around the peak of the flood and deposition during the receding limb observed by camera 2 are broadly similar to the patterns observed at point C in the model. The observations from camera 2 also showed the disconnect between intra-flood changes and net flood changes that was predicted by the model. Although our modelling suggests that width variations alone could drive intra-flood erosion and aggradation in the Daan River gorge, the gorge did not exhibit the approximately symmetric spatial pattern of net flood changes that is predicted by the modelling. This may reflect ongoing adjustment of the channel to uplift and gorge formation. It is also likely that other factors such as flow hydrodynamics, backwater effects or upstream avulsions could also be influencing sediment flux into and through the gorge. Our model results raise the possibility that upstream avulsions are linked to width variations, as tendency for sediment deposition upstream of the gorge during high discharge may increase the

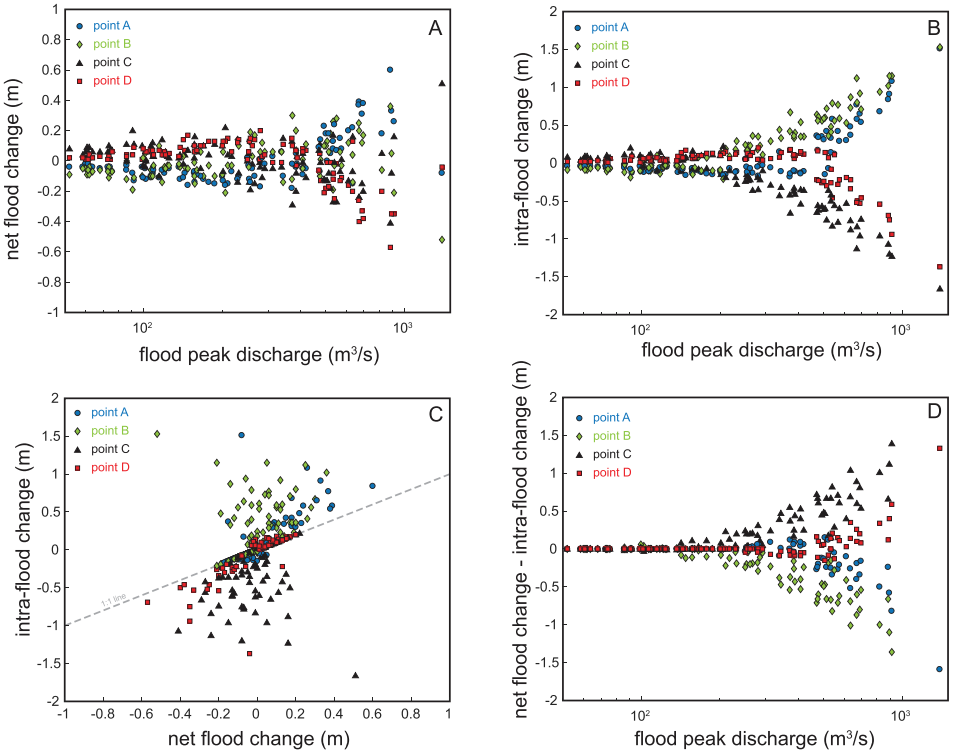

Figure 9. Modelled flood changes. All results shown are for a grain size of 5 cm and combine results from two model runs with discharge time series A and B, making a total of 100 floods. Positive change indicates deposition and negative change indicates erosion. (A) Net flood change versus peak flood discharge. (B) Intra-flood change versus peak flood discharge. (C) Net flood change versus intra-flood change. The 1:1 line is shown in grey. (D) Difference between the net flood change and intra-flood change versus peak flood discharge. [Colour figure can be viewed at wileyonlinelibrary.com]

likelihood of avulsions of the active channel during large floods.

The variability of bedload transport capacity with channel width and discharge has a number of implications for fluvial dynamics, monitoring, modelling and engineering. The response of a channel with variable width depends on the entire hydrograph, not just on the flood peak. Therefore, modelling studies that use uniform discharge or a step function discharge will miss these dynamics. Our modelling also illustrates the importance of flood sequencing and variability of flood magnitude, as a channel will eventually adjust to a repeating flood of uniform size.

Our theoretical analysis highlights the potential importance of retaining the hydraulic radius in bedload transport calculations. Because the hydraulic radius results in equations that are not amenable to analytical solutions, it is common to assume width/depth ratios in a certain range, so that the hydraulic radius can be approximated and cast in a more tractable form. While this may be reasonable for many rivers, care must be taken that the width/depth ratio assumptions are not violated throughout the parameter space of interest. As illustrated in Figure 3, a wide channel assumption that uses flow depth as an approximation for hydraulic radius results in bedload transport estimates that increasingly diverge from transport estimates calculated using the hydraulic radius at large discharges or narrow widths. For a channel of a given width, the wide channel approximation may be reasonable at low and intermediate discharges, but will increasingly overestimate bedload transport as discharge increases. For bedrock-confined rivers that experience a wide range of discharge, this may be a particular problem, as they are likely to experience a range of width/depth ratios throughout the course of a hydrograph, potentially causing hydraulic radius approximations to become inappropriate. For rivers that are bounded by floodplains, the performance of hydraulic radius approximations may depend on the width/depth ratios at bankfull conditions in each of the channel segments.

While our results focus on short-term dynamics of bedload flux, they have potential implications for longer term fluvial erosion. In order for a river to incise bedrock, the bedrock must become exposed to impact by coarse sediment. In many rapidly eroding mountain ranges, rivers are experiencing long-term incision, but riverbeds contain substantial alluvial cover at most times and bedrock is rarely observed (e.g., Tinkler and Wohl, 1998; Yanites *et al.*, 2011). In such systems, controls on the temporal and spatial distribution of coarse sediment cover become important for determining the temporal and spatial patterns of bedrock erosion. Our modelled bed elevations show that at some point during the sequence of floods each portion of the channel experienced erosion such that the sediment elevation lowered below its starting value (Figure 7). As a result, the fluctuations in sediment transport rates that result from width variations could lead to intermittent bedrock exposure in the channel bed, allowing bedrock erosion to occur. This would drive incision in different segments of the channel during different segments of the hydrograph, potentially leading to more frequent and therefore perhaps faster bedrock incision on timescales spanning many floods.

Both our field observations and our modelling results illustrate the potential importance of intra-flood changes in bed elevation or sediment depth. Such changes are typically very difficult to observe, and our modelling suggests that with larger flood size these changes become both more significant and more disconnected from easily observable before/after changes (Figure 9). This may be of particular importance when using observations of alluvial cover depth or distribution during low flow to predict bedrock exposure to erosion during flood events. In addition to potentially affecting bed erosion, bed elevation changes may also influence the location of lateral erosion of channel walls, as lateral bedload impacts and

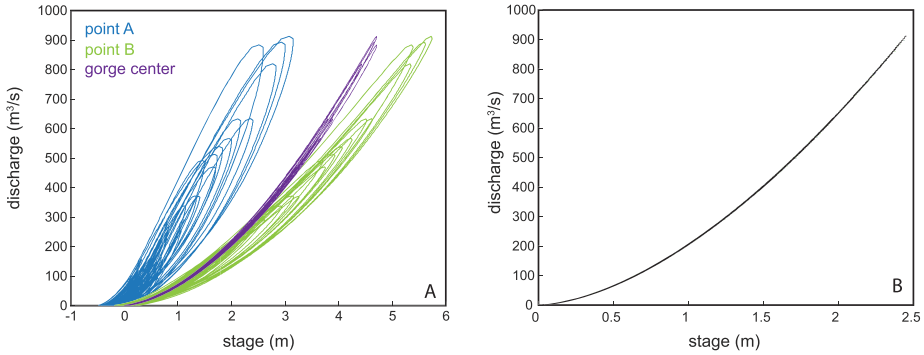

Figure 10. Modelled stage–discharge relationships. Stage is the water surface elevation relative to the initial bed elevation for each point. (A) Stage versus discharge for discharge time series A and a grain size of 5 cm. (B) Stage versus discharge for the uniform channel control case. As this channel experiences no change, the stage–discharge relationship is uniform both spatially and temporally. [Colour figure can be viewed at wileyonlinelibrary.com]

therefore erosion are concentrated to a narrow zone above the bed (e.g., Turowski *et al.*, 2008; Beer *et al.*, 2016; Fuller *et al.*, 2016; Mishra *et al.*, 2018).

Another consequence of intra-flood bed elevation changes is a scattered stage–discharge relationship, as observed in our model results (Figure 10). Each flood is associated with a hysteresis loop of different size, leading to a range of discharges for a given water level. This causes problems for the use of water-level measurements and rating curves to monitor discharge, and may become a significant source of error for discharge gauging and suspended sediment flux calculations in channels with variable width and discharge. While changes to the channel bed can be measured before and after floods, our modelling shows that this is a poor predictor of the bed changes that may have taken place during the flood. Without a way to measure water depth (rather than water surface elevation) or bed elevation during a flood, it may be impossible to accurately measure flood discharge in rapidly varying channels. The location of the gauge relative to a change in width will influence the magnitude of this effect, and may be a consideration for locating water-level gauges. Our modelling suggests that the reaches most likely to be strongly influenced are wide sections near the transition to or from narrow sections (i.e., points A and D in Figure 5). In the narrowest channel sections, the increase in water depth with increasing discharge is greater, so a change in bed elevation is a smaller percentage of the change in water surface elevation. If the width effect is the primary driver of sediment transport variability, then the location of least change over a single flood is predicted to be the centre of the narrow reach (Figure 10). As this reach adjusts its slope in response to changing relative transport capacity, the bed elevation changes should be roughly symmetric, pivoting across a point of minimum change in the centre of the narrow reach.

We intentionally used a simple model in order to isolate the impact of width variation. In doing so, we ignored many aspects of natural systems that will also influence bedload transport. We did not include other sources of variability such as grain size, bed roughness or feedbacks between width and bed configuration (i.e., Golly *et al.*, 2019; Saletti and Hassan, 2020). We also used a constant dimensionless critical shear stress, although it has been shown that this may vary depending on prior conditions (Reid *et al.*, 1985; Masteller *et al.*, 2019; Ockelford *et al.*, 2019). The modelling represents a setting such as Taiwan where large amounts of sediment are transported, with frequent floods well above the threshold of motion. We did not allow the channel to modify its width, on the assumption that the timescale of sediment redistribution is much shorter than the timescale for width adjustment, which is reasonable for bedrock-confined channels (Turowski, 2020). We are interested in the short-term dynamics of the system rather than a steady-state form. We also did not model the flow hydrodynamics, which can become particularly important at the boundaries between reaches of different width, as has been observed in the canyons of the Fraser River by Venditti *et al.* (2014). We did not allow width to vary with flow depth or the flow to overspill the banks. Despite the model's simplicity, we observe a great deal of complexity in sediment flux and bed dynamics, suggesting that width differences alone can drive substantial variations in sediment flux and bed response. In natural systems with additional sources of variability, such as those outlined above, patterns of bedload flux may become even more complicated.

Conclusions

We show that the relative bedload transport capacity of wide versus narrow reaches depends on discharge. The magnitude of the width effect on bedload transport capacity depends on a combination of slope, grain size, the ratio of width in the different reaches and discharge variability. For a given set of conditions, we expect the magnitude of the effect to increase with increasing discharge variability. A simple model of bedload transport in a variable-width channel shows that width difference alone can drive continual bed adjustment in bedrock–alluvial rivers subject to variable flood sizes. These relationships between width, discharge and bedload flux can lead to highly dynamic rivers, with implications for stage–discharge relationships, sediment flux estimates, distribution of alluvial cover and bedrock erosion. Our analysis highlights the potential for bedload transport variability throughout the course of individual floods, and the importance of using full hydrographs in modelling bedload dynamics.

Acknowledgements—Fieldwork in Taiwan was supported by Taiwan NSC grant 2811-M-002-092 and National Taiwan University. KLC thanks former postdoc advisor John Suppe for support, as well as Po-Nong Li and Chia-Yu Chen for assistance in the field. We thank two anonymous reviewers for their constructive feedback.

Data Availability Statement

The sedFlow model is available from the Swiss Federal Institute for Forest, Snow and Landscape Research WSL (https://www.wsl.ch/de/services-und-produkte/software-websites-und-apps/sedflow.html). The Daan River data are available on request.

Conflicts of Interest

The authors declare no conflicts of interest.

References

Beer AR, Turowski JM, Kirchner JW. 2016. Graffiti for science: erosion painting reveals spatially variable erosivity of sediment-laden flows. *Earth Surface Dynamics Discussions* **4**(4): 885–894. https://doi.org/10.5194/esurf-2016-27

Bull WB. 1979. Threshold of critical stream power in streams. *Geological Society of America Bulletin* **90**: 453–464.

Bursztyn N, Pederson JL, Tressler C, Mackley RD, Mitchell KJ. 2015. Rock strength along a fluvial transect of the Colorado Plateau: quantifying a fundamental control on geomorphology. *Earth and Planetary Science Letters* **429**: 90–100.

Carson MA, Griffiths GA. 1987. Influence of channel width on bed load transport capacity. *Journal of Hydraulic Engineering* **113**(12): 1489–1508.

Church M. 2006. Bed material transport and the morphology of alluvial river channels. *Annual Review of Earth and Planetary Sciences* **34**: 325–354.

Cook KL, Turowski JM, Hovius N. 2013. A demonstration of the importance of bedload transport for fluvial bedrock erosion and knickpoint propagation. *Earth Surface Processes and Landforms* **38**(7): 683–695.

Cook KL, Turowski JM, Hovius N. 2014. River gorge eradication by downstream sweep erosion. *Nature Geoscience* **7**: 682–686. https://doi.org/10.1038/NGEO2224

Davies T, Lee AL. 1988. Physical hydraulic modelling of width reduction and bed level change in braided rivers. *Journal of Hydrology, New Zealand* **27**: 113–127.

Eaton BC, Church M. 2007. Predicting downstream hydraulic geometry: a test of rational regime theory. *Journal of Geophysical Research: Earth Surface* **112**(F3). https://doi.org/10.1029/2006JF000734

Fernandez-Luque R, van Beek R. 1976. Erosion and transport of bedload sediment. *Journal of Hydraulic Research* **14**(2): 127–144.

Finnegan NJ, Sklar LS, Fuller TK. 2007. Interplay of sediment supply, river incision, and channel morphology revealed by the transient evolution of an experimental bedrock channel. *Journal of Geophysical Research* **112**: F03S11. https://doi.org/10.1029/2006JF000569

Fuller TK, Gran KB, Sklar LS, Paola C. 2016. Lateral erosion in an experimental bedrock channel: the influence of bed roughness on erosion by bed load impacts. *Journal of Geophysical Research: Earth Surface* **121**(5): 1084–1105.

Golly A, Turowski JM, Badoux A, Hovius N. 2019. Testing models of step formation against observations of channel steps in a steep mountain stream. *Earth Surface Processes and Landforms* **44**: 1390–1406. https://doi.org/10.1002/esp.4582

Gomez B. 1983. Temporal variations in bedload transport rates: the effect of progressive bed armouring. *Earth Surface Processes and Landforms* **8**(1): 41–54.

Gomez B. 1991. Bedload transport. *Earth-Science Reviews* **31**(2): 89–132.

Gomez B, Naff RL, Hubbell DW. 1989. Temporal variations in bedload transport rates associated with the migration of bedforms. *Earth Surface Processes and Landforms* **14**(2): 135–156.

Griffiths GA, Carson MA. 2000. Channel width for maximum bedload transport capacity in gravel-bed rivers, South Island, New Zealand. *Journal of Hydrology, New Zealand* **39**: 107–126.

Habersack HM, Nachtnebel HP, Laronne JB. 2001. The continuous measurement of bedload discharge in a large alpine gravel bed river. *Journal of Hydraulic Research* **39**(2): 125–133.

Heimann FUM, Rickenmann D, Turowski JM, Kirchner JW. 2015a. SedFlow: a tool for simulating fractional bedload transport and longitudinal profile evolution in mountain streams. *Earth Surface Dynamics* **3**(1): 15–34. https://doi.org/10.5194/esurf-3-15-2015

Heimann FUM, Rickenmann D, Böckli M, Badoux A, Turowski JM, Kirchner JW. 2015b. Calculation of bedload transport in Swiss mountain rivers using the model sedFlow: proof of concept. *Earth Surface Dynamics* **3**: 35–54. https://doi.org/10.5194/esurf-3-35-2015

Hoey T. 1992. Temporal variations in bedload transport rates and sediment storage in gravel-bed rivers. *Progress in Physical Geography* **16**(3): 319–338.

Korup O. 2005. Geomorphic imprint of landslides on alpine river systems, southwest New Zealand. *Earth Surface Processes and Landforms* **30**: 783–800.

Kuhnle RA. 1992. Bed load transport during rising and falling stages on two small streams. *Earth Surface Processes and Landforms* **17**(2): 191–197.

Lavé J, Avouac JP. 2001. Fluvial incision and tectonic uplift across the Himalayas of central Nepal. *Journal of Geophysical Research* **106**: 26,526–26,591. https://doi.org/10.1029/2001JB000359

Liu Z, Todini E. 2002. Towards a comprehensive physically-based rainfall-runoff model. *Hydrology and Earth System Sciences* **6**: 859–881. https://doi.org/10.5194/hess-6-859-2002

Mackin JH. 1948. Concept of the graded river. *Geological Society of America Bulletin* **59**: 463–512.

Mao L, Dell'Agnese A, Huincache C, Penna D, Engel M, Niedrist G, Comiti F. 2014. Bedload hysteresis in a glacier-fed mountain river. *Earth Surface Processes and Landforms* **39**(7): 964–976.

Masteller CC, Finnegan NJ, Turowski JM, Yager EM, Rickenmann D. 2019. History dependent threshold for motion revealed by continuous bedload transport measurements in a steep mountain stream. *Geophysical Research Letters* **46**: 2583–2591.

Meade RH. 1985. Wavelike movement of bedload sediment, East Fork River, Wyoming. *Environmental Geology and Water Sciences* **7**(4): 215–225.

Mishra J, Inoue T, Shimizu Y, Sumner T, Nelson JM. 2018. Consequences of abrading bed load on vertical and lateral bedrock erosion in a curved experimental channel. *Journal of Geophysical Research: Earth Surface* **123**(12): 3147–3161.

Montgomery DR, Gran KB. 2001. Downstream variations in the width of bedrock channels. *Water Resources Research* **37**: 1841–1846.

Mueller DS, Wagner CR. 2005. *Field observations and evaluations of streambed scour at bridges* (No. FHWA-RD-03-052). US Federal Highway Administration, Office of Research, Development, and Technology: McLean, VA.

Nanson GC. 1974. Bedload and suspended-load transport in a small, steep, mountain stream. *American Journal of Science* **274**(5): 471–486.

Ockelford A, Woodcock S, Haynes H. 2019. The impact of inter-flood duration on non-cohesive sediment bed stability. *Earth Surface Processes and Landforms* **44**(14): 2861–2871.

Ouimet WB, Whipple KX, Crosby BT, Johnson JP, Schildgen TF. 2008. Epigenetic gorges in fluvial landscapes. *Earth Surface Processes and Landforms* **33**(13): 1993–2009.

Recking A, Frey P, Paquier A, Belleudy P, Champagne JY. 2008. Feedback between bed load transport and flow resistance in gravel and cobble bed rivers. *Water Resources Research* **44**(5): W05412.

Reid I, Frostick LE, Layman JT. 1985. The incidence and nature of bedload transport during flood flows in coarse-grained alluvial channels. *Earth Surface Processes and Landforms* **10**: 33–44.

Richardson EV, Davis SR. 1995. *Evaluating scour at bridges* (No. HEC 18). US Federal Highway Administration, Office of Technology Applications: Washington, DC.

Rickenmann D. 2001. Comparison of bed load transport in torrents and gravel bed streams. *Water Resources Research* **37**: 3295–3305.

Roth DL, Finnegan NJ, Brodsky EE, Cook KL, Stark CP, Wang HW. 2014. Migration of a coarse fluvial sediment pulse detected by hysteresis in bedload generated seismic waves. *Earth and Planetary Science Letters* **404**: 144–153.

Saletti M, Hassan MA. 2020. Width variations control the development of grain structuring in steep step-pool dominated streams: insight from flume experiments. *Earth Surface Processes and Landforms* **45** (6): 1430–1440.

SCS. 1972. *National Engineering Handbook, Section 4: Hydrology*. Soil Conservation Service, USDA: Washington, DC.

Sklar LS, Dietrich WE. 2004. A mechanistic model for river incision into bedrock by saltating bed load. *Water Resources Research* **40**: W06301. https://doi.org/10.1029/2003WR002496

Sturm TW, Ettema R, Melville BW. 2011. *Evaluation of Bridge-Scour Research: Abutment and Contraction Scour Processes and Prediction*.

National Cooperative Highway Research Program, Transportation Research Board of the National Academies: Washington, DC; 24–27.

Tinkler KJ, Wohl EE. 1998. A primer on bedrock channels. In *Rivers Over Rock: Fluvial Processes in Bedrock Channels*, Tinkler KJ, Wohl EE (eds), Geophysical Monograph Series 107. American Geophysical Union: Washington, DC; 1–18.

Turowski J. 2020. Mass balance, grade, and adjustment timescales in bedrock channels. *Earth Surface Dynamics* **8**: 103–122.

Turowski JM, Hovius N, Hsieh M-L, Lague D, Chen M-C. 2008. Distribution of erosion across bedrock channels. *Earth Surface Processes and Landforms* **33**: 353–363. https://doi.org/10.1002/esp.1559

Turowski JM, Yager EM, Badoux A, Rickenmann D, Molnar P. 2009. The impact of exceptional events on erosion, bedload transport and channel stability in a step-pool channel. *Earth Surface Processes and Landforms* **34**(12): 1661–1673.

Turowski JM, Badoux A, Leuzinger J, Hegglin R. 2013. Large floods, alluvial overprint, and bedrock erosion. *Earth Surface Processes and Landforms* **38**: 947–958. https://doi.org/10.1002/esp.3341

Venditti JG, Rennie CD, Bomhof J, Bradley RW, Little M, Church M. 2014. Flow in bedrock canyons. *Nature* **513**(7519): 534–537.

Whipple KX. 2004. Bedrock rivers and the geomorphology of active orogens. *Annual Review of Earth and Planetary Sciences* **32**: 151–185. https://doi.org/10.1146/annurev.earth.32.101802.120356

Whitbread K, Jansen J, Bishop P, Attal M. 2015. Substrate, sediment, and slope controls on bedrock channel geometry in postglacial streams. *Journal of Geophysical Research: Earth Surface* **120**(5): 779–798.

Yanites BJ, Tucker GE. 2010. Controls and limits on bedrock channel geometry. *Journal of Geophysical Research* **115**: F04019. https://doi.org/10.1029/2009jf001601

Yanites BJ, Tucker GE, Mueller KJ, Chen YG, Wilcox T, Huang SY, Shi KW. 2010. Incision and channel morphology across active structures along the Peikang River, central Taiwan: implications for the importance of channel width. *Geological Society of America Bulletin* **122**: 1192–1208. https://doi.org/10.1130/B30035.1

Yanites BJ, Tucker GE, Hsu H-L, Chen C, Chen Y-G, Mueller KJ. 2011. The influence of sediment cover variability on long-term river incision rates: an example from the Peikang River, central Taiwan. *Journal of Geophysical Research* **116**: F03016. https://doi.org/10.1029/2010JF001933

